The Sintering Temperature Effect on Magnetocaloric Effect in La$_2$MnNiO$_6$ Double Perovskite Manganite Material

İbrahim Barış SEVER[1], Arda KANDEMİR[2], Ali Osman AYAŞ[3,*], Ahmet EKİCİBİL[4]

[1]*Adıyaman University, Faculty of Science and Letters, Department of Physics, 02040, Adıyaman, Türkiye*
ibrahim.baris02@gmail.com, ORCID: 0000-0001-6745-2472
[2]*Çukurova University, Faculty of Science and Letters, Department of Physics, 01250, Adana, Türkiye*
ardakandemir88@gmail.com, ORCID: 0000-0002-9439-0366
[3]*Adıyaman University, Faculty of Science and Letters, Department of Physics, 02040, Adıyaman, Türkiye*
aayas@adiyaman.edu.tr, ORCID: 0000-0002-6186-8191
[4]*Çukurova University, Faculty of Science and Letters, Department of Physics, 01250, Adana, Türkiye*
ahmetcan@cu.edu.tr, ORCID: 0000-0003-3071-0444

Abstract

La$_2$NiMnO$_6$ double-perovskite manganite samples were produced with sol-gel method to investigate structural, morphological, magnetic and magnetocaloric properties. They were sintered at 1000 and 1100 ˚C for LNM-1000 and LNM-1100 sample, respectively. The crystal structure of the samples was determined as Rhombohedral with R$\overline{3}c$ space group. Morphological analyses revealed that LNM-1000 sample included different polygonal shaped grains with small magnitudes, while grain boundaries became unclear for the LNM-1100 sample. The Curie temperatures were determined as 200 and 220 K while effective magnetic moment values were calculated as 1.75 and 2.13 for LNM-1000 and LNM-1100 samples, respectively. Arrot plots showed that samples exhibited second order magnetic phase transition. Maximum magnetic entropy change and relative cooling power values were calculated as 0.21, 0.25 J kg^{-1} K^{-1} and 46.2, 50.5 J kg^{-1} for LNM-1000 and LNM-1100 samples, respectively. Although the samples have the Curie temperature around sub-room temperature range that is much higher than Gd$_2$NiMnO$_6$

(5 K) and they have second order magnetic phase transition, relatively low value of magnetic entropy change values of these samples limit their usage as a magnetic coolant material.

Keywords: Magnetic refrigeration; Magnetocaloric effect; Curie temperature; Double perovskite manganites.

La$_2$MnNiO$_6$ Çift Katlı Perovskit Manganit Malzemede Sinterleme Sıcaklığının Manyetik Soğutma Parametrelerinin Üzerindeki Etkisi

Öz

La$_2$NiMnO$_6$ çift peroksit manganit örnekleri yapısal, morfolojik, manyetik ve manyetokalorik özelliklerini araştırmak için sol-jel yöntemi ile üretildi. LNM-1000 ve LNM-1100 numuneleri sırasıyla 1000 ve 1100 °C'de sinterlenmişlerdir. Numunelerin kristal yapısı R$\overline{3}$c uzay grubuna sahip Rhombohedral olarak belirlenmiştir. Morfolojik analizler, LNM-1000 numunesinin küçük boyutlara sahip farklı poligonal şekilli taneler içerdiğini, LNM-1100 numunesinde ise tane sınırlarının belirsizleştiğini ortaya koymuştur. Curie sıcaklıkları 200 ve 220 K olarak belirlenirken, etkin manyetik moment değerleri LNM-1000 ve LNM-1100 numuneleri için sırasıyla 1.75 ve 2.13 olarak hesaplanmıştır. Arrot grafikleri örneklerin ikinci dereceden manyetik faz geçişi sergilediğini göstermiştir. Maksimum manyetik entropi değişimi ve bağıl soğutma gücü değerleri LNM-1000 ve LNM-1100 numuneleri için sırasıyla 0.21, 0.25 J kg^{-1} K^{-1} ve 46.2, 50.5 J kg^{-1} olarak hesaplanmıştır. Örneklerin Curie sıcaklığının oda sıcaklığının altında Gd$_2$NiMnO$_6$'dan (5 K) çok daha yüksek olması ve ikinci dereceden manyetik faz geçişine sahip olması gibi avantajlarına rağmen, bu örneklerin manyetik entropi değişim değerlerinin nispeten düşük olması manyetik soğutucu malzeme olarak kullanımlarını sınırlamaktadır.

Anahtar Kelimeler: Manyetik soğutma; Manyetokalorik etki; Curie sıcaklığı; Çift-katmanlı perovskitler.

1. Introduction

Increasing energy demand and energy related environmental problems which adversely affect our health are one of the provocative problems of the modern humanity [1]. Due to this fact, many governments pay considerable attention to reduce these adverse effects [2]. It should be noted that refrigeration devices have relatively high energy consumption rate among other energy consuming technologies with approximately 15% [3] of the total energy consumption rate in the world. Moreover, current refrigeration systems also have some other hazardous effects on the environment like ozone-depleting and/or greenhouse effect [4, 5]. By considering given disadvantages of current cooling devices, many scientists focus on alternative cooling

technologies like magnetic cooling due to possible energy efficiency and environmentally green nature [6-8]. Magnetic cooling technology is mainly based on Magnetocaloric Effect (MCE). For this reason, it is important to define MCE which can be defined as thermal response of magnetic material under the influence of applied magnetic field change [1, 5, 7, 9]. MCE can be measured by adiabatic temperature change (ΔT_{AD}) and/or magnetic entropy change (ΔS_M) [6, 8, 10]. ΔS_M is mainly related to magnetic moment alignment and maximum change of these parameters occurs around the magnetic phase transition temperature [1, 5, 7, 9].

Although many studies about several magnetocaloric material families in the literature report results of the cooling performance parameters of these families, it is not reached an optimization on all parameters yet [7, 9, 11-13]. The closest results of the targeted properties were observed in Gd element and its alloys [14]. On the other hand, Gd element has the high-cost problem that limits its usage as a magnetic coolant materials. Similar handicaps exist in other potential candidate coolant materials and therefore researchers continue to search new candidates. Among these candidates, perovskite manganites reach considerable attention due to exposing rich physical and magnetic properties [1, 15-19]. The general formula of the perovskite manganites is given as $A_{1-x}B_xMnO_3$, where A means rare-earth elements and B for the alkaline earth elements. This stoichiometric structure allows researchers to use this family in very large scale of technological application topics like spintronic devices [20], magnetic sensors [21, 22], and coolants for magnetic refrigeration [16, 23-27].

Perovskite manganites have also a slightly different form than $A_{1-x}B_xMnO_3$ type called double perovskite manganite and the chemical formula of this type is given as $A_{2-x}B_xMn_2O_6$ [15, 24, 25, 28]. Although a lot of Research about $A_{1-x}B_xMnO_3$ type perovskites have been performed, research about $A_{2-x}B_xMn_2O_6$ type double perovskite is relatively rare. Physical mechanism about this form should be explained and extra data about the sintering treatment is needed by characterizing some new and novel members. Due to this reason, in this work we have produced La_2MnNiO_6 sample under two different sintering temperature. The morphological, structural, magnetic, and magnetocaloric properties of this novel compound were characterized and explained in detail. Previous studies about this structure have reported some properties like photocatalytic activity, adsorption of mono-crotophos from aqueous environment etc., but as far as we know, there is no report in the literature that investigate all these properties. Additionally, sintering temperature effect on this structure was also investigated firstly in this work. The result of this study can yield useful understandings to obtain room temperature range magnetocaloric materials for magnetic cooling applications.

2. Experimental Procedure

Polycrystalline La_2MnNiO_6 Double perovskite manganite sample was sol-gel method. To obtain sample with desired stoichiometry required quantities of $La(NO_3)_3 \cdot xH_2O$ (99.9% purity), NiO (99.9% purity) and MnO_2 ($\geq$99% purity). Monoethylene glycol with 99.9% purity, Hydrochloric acid with 37 % purity, nitric acid with 70 % purity, and citric acid monohydrate with 99.9% purity were used as a chelating substance. All materials were heated and mixed by magnetic stirrer at 300 ˚C. This process continues to obtain gel-like precipitation. This form was burned at 500 ˚C for 1 h, then calcined at 600 ˚C for 6 h. To obtain fine powders, the obtained materials were grounded by an agate mortar. After this process, powder samples were pressed to make disc-shaped samples. Then, disc-shaped samples were sintered at 1000 and 1100 ˚C for 24 h in the air and these samples are labelled as LNM-1000 and LNM-1100, respectively.

The crystal structure of the samples was performed with X-Ray Diffraction (XRD) method. The CuKα with λ=1.5406 Å at room temperature was used as radiation source. X'Pert High Score Plus software was used to determine potential candidate structure and the Rietveld refinement method ready in Fullprof software was used to determine the crystal structure of the samples. Morphological properties of the samples were analyzed by Scanning Electron Microscope (SEM) technique. Elemental analyses of the samples were performed by Energy Dispersive X-Ray Spectroscopy (EDS) method.

The magnetic properties of the samples have been analyzed by two measurements called temperature dependent *M(T)* and isothermal magnetization curves *M(H)* measurements. These measurements performed with a Vibration Sample Magnetometer (VSM) equipped Physical Properties Measurement System (PPMS). The *M(T)* of the samples measured from 10 to 350 K temperature range under two regimes called zero-field cooled (ZFC) and field-cooled (FC). *M(H)* curves performed from 0 to 5 T magnetic field at 4 K temperature steps around phase transition temperature region. All measurements, analyzes, methods and techniques were carried out at Çukurova University Central Research Laboratory (ÇÜMERLAB).

3. Results and Discussions

The crystallographic information of the samples was investigated by using XRD data collected at room temperature. The Rietveld's refinement method [29] via Fullprof software has been used to analyze XRD data [30]. The refinement results are given in the Figs.1a-b for LNM-1000, LNM-1100 samples, respectively. The parameters about crystal structure obtained from the refinement analysis are tabulated in Table 1.
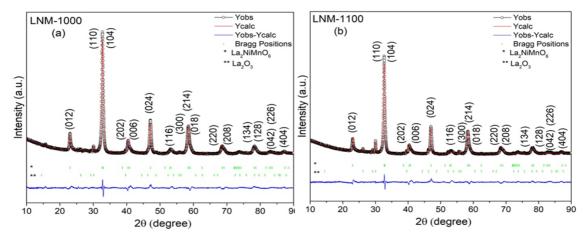
Figure 1: XRD Patterns for samples (a) LNM-1000, (b) LNM-1100. The red line, black circle, green bars, blue line, and asterisk represent calculated data, observed data, Bragg positions, differences between observed and calculated data, and impurity phases, respectively

Table 1: The structural parameters for samples LNM-1000 and LNM-1100 samples. The lattice parameters (*a*, *b*, *c*), unit cell volume (V), average bond angle of B-O-B (B: Mn, Ni), the average bond length of B-O (B: Mn, Ni), the crystallite size (D), and the convergence factor (χ^2) values for each sample

Structural Parameters	Samples	
	LNM-1000	**LNM-1100**
a (Å)	5.4743	5.4858
b (Å)	5.4743	5.4858
c (Å)	13.2607	13.2938
V (Å³)	344.1534	346.4652
<B-O-B> (°)	156.13	153.80
<d_{B-O}> (Å)	1.92861	1.93942
D (nm)	21.74	24.04
χ^2	3.97	3.93

The convergence between theoretical model and observed data known as chi-squared (χ^2) observed from Rietveld refinement for LNM-1000 and LNM-1100 samples are 3.83 and 3.60, respectively. These results mean (χ^2<4) observed and experimental data well match with each other. From this result, it can be argued that these samples have rhombohedral structure with R$\overline{3}c$ space group. However, small amount of impurity phase belongs to La_2O_3 structure also detected. The main crystal structure kept unchanged by increasing sintering temperature (T_S) from 1000 °C to 1100 °C. As can be seen from Table 1, the lattice parameters increased by increasing T_S. The change of lattice parameters inevitably affected the average B-O bond length and average B-O-B bond angle (B: Mn, Ni) (See Table 1).

For magnetic and magnetocaloric properties the crystallite size (D) plays an important role due to the indirect result of determining boundary lines that is known non-magnetic places in materials. For this reason, calculating D parameter is important and can be calculated by Debye-Scherrer equation given below [31, 32]:

$$D = \frac{\kappa\lambda}{\beta cos\theta} \tag{1}$$

where λ is the wavelength of the x-ray ($\lambda_{Cu-K\alpha}$ = 1.5406 Å), κ is the crystallite shape factor (0.94 for each sample), and β is the peak full width at half maximum at the observed peak angle θ (in radians). It can be seen from Table 1 that the average crystallite size value increases by increasing T_S. This increment is consistent with the results obtained from the literature [33-36] and may be due to the higher growth rate of crystallite size at higher temperatures below melting point [35, 36].

To investigate morphological and elemental properties of the samples SEM and EDS methods had been used. SEM images with EDS spectra graphs for LNM-1000 and LNM-1100 samples are given in Figs.2 (a-b).
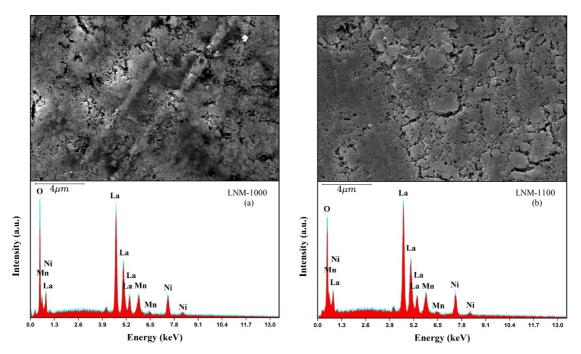

Figure 2: SEM images and EDS measurements for samples (a) LNM-1000, (b) LNM-1100

As can be seen from the SEM photo in the Fig. 2a, grains have different polygonal shapes with quite small magnitudes. In some places, small amount of aggregation that indicates liquid phase [24], is detected. By increasing T_S, the boundary lines become unclear that can be

interpreted as areas which includes liquid phase increases by increasing T_S. The liquid phase may play a role to get grains together that might be the reason of unclear boundary lines in LNM-1100 sample [24]. From EDS spectra, it is understood that both samples include all starting elements that means no element loss during preparation process and there is no impurity element in both samples.

Temperature dependent magnetization measurements *(M(T))* of LNM-100 and LNM-1100 samples measured in FC and ZFC modes were carried out under 25 mT external magnetic field to examine the magnetic behavior and to determine the phase transition temperatures. The results are shown in Figs. 3 (a-b) (left axes).
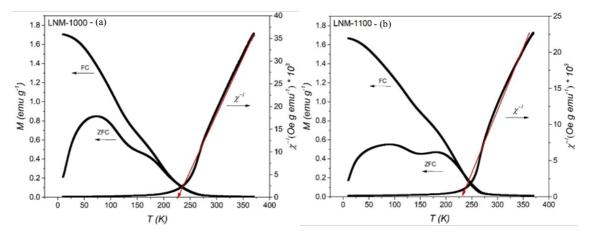

Figure 3: The *M* (*T*) curves obtained at both FC and ZFC modes and inverse susceptibility for (a) LNM-1000 and (b) LNM-1100 samples

It can be seen from left axes of the Figs. 3 (a-b) magnetization of the samples decreases by increasing the temperature in FC mode. On the other hand, in ZFC mode, magnetization behavior is different at low temperature range where the magnetization increases at first and then starts to decrease by increasing temperature. Magnetization closes to zero value in both FC and ZFC mode at high temperature region. This behavior means magnetic phase transition from ferromagnetic to paramagnetic phase. Difference between ZFC and FC mode at low temperature range indicates existence of antiferromagnetic interaction, domain wall pinning effect and the spin-class like behavior in the matrix of the samples. Maximum magnetic entropy change occurs at the magnetic phase transition temperature T_C. For this reason, determining T_C is important and in this work, we have used two methods to determine it. At the first method, inverse susceptibility cure is used. Red straight line that is fitting the paramagnetic part of the graphs cuts the x axes at T_C. In the second method, we have used dM/dT graphs given in Figs 4 (a-b).
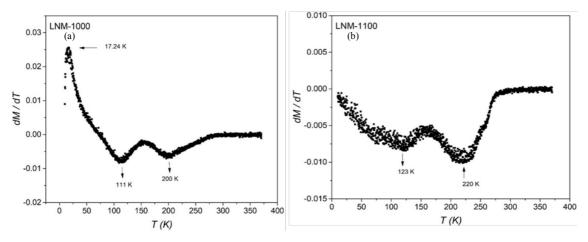
Figure 4: The *dM/dT*-(*T*) curves for (a) LNM-1000 and (b) LNM-1100 samples

The minimum point of the dM/dT graphs called as TC. Determined TC values of the samples are tabulated in Table 2. As can be seen from the Table 2, TC values are 200 and 220 K for LNM-1000 and LNM-1100, respectively. The increase in TC may come from decreasing boundary lines of grains that is also seen in SEM images as increasing aggregated areas. Boundary lines are known magnetically inactive places and decreasing this kind of areas leads to increase in magnetic nature of the sample and for this reason, TC value of the sample increases. To compare the phase transition temperatures of the samples, the phase transition temperature of the Gd2NiMnO6 [37] sample was also gift in Table 2. It can be seen from the Table 2, TC values of the samples increase considerably with change of Gd with La. The TC values obtained from inverse susceptibility curves show very small differences that comes from antiferromagnetic interaction explained above. This fact can also be seen as a difference between inverse susceptibility curve of paramagnetic side and the red line extrapolated in this area. This discrepancy comes from co-existence of paramagnetic, ferromagnetic and/or antiferromagnetic clusters in this temperature range which is called Griffiths phase [38].

Another important magnetic parameter is effective magnetic moment (μ_{eff}). Left axes of the Figs.3 show linear behavior at high temperature range. This part can be fitted to Curie-Weiss law and μ_{eff} can be calculated by this law given as:

$$\chi = \frac{C}{T - \theta} \tag{2}$$

where θ is the paramagnetic curie temperature, C is the Curie constant and this value for the samples can be given as:

$$C = \frac{N\mu_{eff}^2\mu_B^2}{3k_B} \tag{3}$$

where μ_B is the Bohr magneton, N is Avogadro's number, k_B is Boltzmann constant, and μ_{eff} is the effective magnetic moment. By using given relations above, μ_{eff} values are calculated and tabulated in Table 2. As can be seen from Table 2, μ_{eff} value increases by increasing T_S that supports the strengthening of the magnetic nature of the samples.

Table 2: Magnetic and magnetocaloric parameters of the LNM-1000 and LNM-1100 samples

Sample	T_C (K)	$\mu_{eff}(\mu_B)$	$-\Delta S_M$ (J kg⁻¹K⁻¹)	RCP (J kg⁻¹)	Reference
LNM-1000	200	1.75	0.21	46.2	This work
LNM-1100	220	2.13	0.25	50.5	This work
Gd₂NiMnO₆	5	-	26	-	[33]

Another measurement to investigate magnetic properties is isothermal magnetization curves (*M(H)*) that measured up to 5 T magnetic fields around phase transition range with 4 K temperature steps. Measured *M(H)* curves are given in Figs. 5.
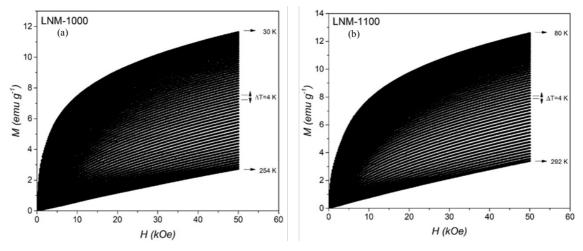

Figure 5: Isothermal magnetization curves measured at various temperatures around T_C with a step of 4 K for (a) LNM-1000 and (b) LNM-1100 samples

It can be seen from the Figs.5 (a-b) that magnetization curves increase suddenly by increasing the applied magnetic field at low temperature measurements. These curves close to linear behavior for measurements at measured high temperature side. This behavior indicates magnetic phase transition from ferromagnetic (FM) to paramagnetic (PM) phase that is also observed in *M(T)* part. In all curves saturation is not reached that may come from such parameters

like short-range FM interaction, magnetic inhomogeneity or low level of applied magnetic field [39].

To determine the magnetic cooling capacity of a magnetic material, magnetic entropy change parameter is a frequently used parameter and can be calculated with using isothermal magnetization curves and Eqn. (4) given below. Application of this equation explained anywhere else [1, 5]

$$-\Delta S_M = \int_0^H \left(\frac{\partial M}{\partial T}\right)_H dT \tag{4}$$

The $-\Delta S_M$-T curves obtained from Eqn. (4) are given in Figs. 6 (a-b) and maximum ΔS_M values are also listed in Table 2.
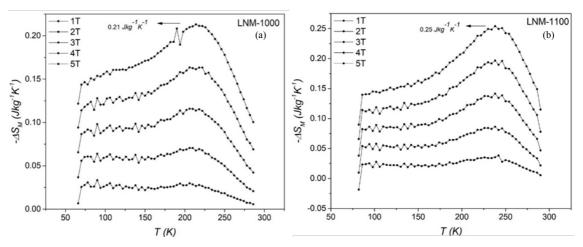

Figure 6: $-\Delta S_M$-(T) curves for (a) LNM-1000 and (b) LNM-1100 samples

As can be seen also in other magnetic properties, $-\Delta S_M$ value increases with increasing T_S value (see Table 2). This increase in magnetic nature of the samples can be explained with increasing aggregated sites which leads to increase the active magnetic field in samples. It can be said that maximum $-\Delta S_M$ value of the samples is quite low level when the result is compared with the Gd based example given in Table 2. This result limits the usage of these samples as magnetic coolant material. It should be noted that keeping $-\Delta S_M$ value of the samples at high level as in Gd based example is important while the T_C value is increased.

Reversible magnetic phase transition is another important parameter that is expected from a candidate coolant material. Magnetic materials that show second order magnetic phase transition also exhibit negligible thermal and magnetic hysteresis and vice versa for materials that exhibit first order magnetic phase transition type. Banerjee's criterion is the known method of

determining the magnetic phase transition type of materials [40]. In this method, H/M vs M^2 graph called Arrot plot obtained from *M(H)* data is used to determine magnetic phase transition nature of the samples. Obtained graphs are given in Figs. 7 (a-b).
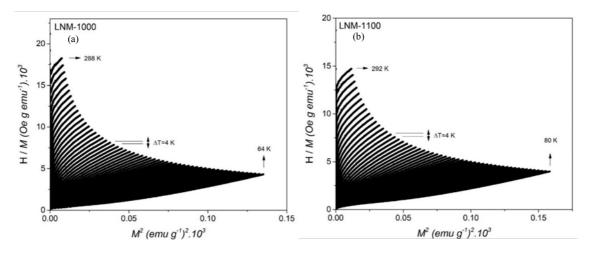

Figure 7: Arrott plots for (a) LNM-1000 and (b) LNM-1100 samples.

According to Arrot graphs, the slope of the curves is positive that indicates that the samples have second order magnetic phase transition nature. Due to this property, ignorable thermal and magnetic hysteresis accommodate to the magnetic phase transition of the samples that makes these samples more suitable for magnetic cooling applications.

Relative Cooling Power (RCP) is also an important parameter for MCE and is calculated by equation below:

$$RCP = -\Delta S_M^{max} x \, \delta T_{FWHM} \tag{5}$$

where δT_{FWHM} is the full width at half maximum of the $-\Delta S_M(T)$ curve. In ideal thermodynamic cycle the amount of heat that can be transferred between heat and cold sides could be represented by RCP. The RCP values calculated under $\Delta H = 5$ T are listed in Table 2. As also in other parameters, the RCP value increases with increasing T_S.

4. Conclusion

As a conclusion, LNM-1000 and LNM-1100 samples were produced with sol-gel method successfully and their structural, magnetic, and magnetocaloric properties were also characterized. From the Rietveld's refinement method, crystal structure of the samples was determined as Rhombohedral structure with R$\overline{3}$c space group. LNM-1000 sample has quite small, different polygonal shaped grains with clear grain boundaries and by increasing temperature, in

the LNM-1100 sample, areas that have a melting form of the grains increases which means grain boundaries are not seen clearly in these areas. Both samples show a second-order magnetic phase transition from ferromagnetic to paramagnetic phase by increasing temperature. T_C values were determined as 200 and 220 K for LNM-1000 and LNM-1100 samples, respectively. $-\Delta S_M^{max}$ and RCP values were calculated as 0.21, 0.25, and 46.2, 50.5 for the LNM-1000 and LNM-1100 samples, respectively.

By considering the magnetic cooling results of the samples and Gd_2NiMnO_6 sample, obtaining magnetic cooling samples that exhibit second order magnetic phase transition at high temperature range is acceptable. On the other hand, in future works, it should be investigated some substitution effects to increase the $-\Delta S_M^{max}$ values of the samples while keeping or increasing T_C values. From the results of the samples, it can be said that increasing particle and grain sizes mainly has a positive effect on the magnetocaloric effect parameters of the samples.

Acknowledgments

References

[1] Ayaş, A.O., Kılıç Çetin, S., Akça, G., Akyol, M., Ekicibil, A., *Magnetic refrigeration: current progress in magnetocaloric properties of perovskite manganite materials*, Materials Today Communications, 35, 105988, 2023.

[2] Gross, R., Leach, M., Bauen, A., *Progress in renewable energy*, Environment International, 29,105-122, 2003.

[3] Tassou, S.A., Ge, Y., Hadawey, A., Marriott, D., *Energy consumption and conservation in food retailing*, Applied Thermal Engineering, 31, 147-156, 2011.

[4] Gschneidner Jr, K.A., Pecharsky, V.K., Pecharsky, A.O., Zimm, C.B., *Recent developments in magnetic refrigeration*, Materials Science Forum, 315-317, 69-76, 1999.

[5] Ayaş, A.O., Akyol, M., Ekicibil, A., *Structural and magnetic properties with large reversible magnetocaloric effect in (La_{1-x}Pr_x)_{0.85}Ag_{0.15}MnO₃ (0.0 ≤ x ≤ 0.5) compounds*, Philosophical Magazine, 96, 922-937, 2016.

[6] Gschneidner Jr, K.A., Pecharsky, V.K., Tsokol, A.O., *Recent developments in magnetocaloric materials,* Reports on Progress in Physics, 68, 1479, 2005.

[7] Phan, M.-H., Yu, S.-C., *Review of the magnetocaloric effect in manganite materials*, Journal of Magnetism and Magnetic Materials, 308, 325-340, 2007.

[8] Gutfleisch, O., Willard, M.A., Brück, E., Chen, C.H., Sankar, S.G., Liu, J.P., *Magnetic materials and devices for the 21st century: stronger, lighter, and more energy efficient*, Advanced Materials, 23, 821-842, 2011.

[9] Gschneidner Jr, K.A, Pecharsky, V.K., *Magnetocaloric materials*, Annual Review of Materials Science, 30, 387-429, 2000.

[10] Zhang, Y., Tian, Y., Zhang, Z., Jia, Y., Zhang, B., Jiang, M., Wang, J., Ren, Z., *Magnetic properties and giant cryogenic magnetocaloric effect in B-site ordered antiferromagnetic Gd_2MgTiO_6 double perovskite oxide*, Acta Materialia, 226, 117669, 2022.

[11] Ram, N.R., Prakash, M., Naresh, U., Kumar, N.S., Sarmash, T.S., Subbarao, T., Kumar, R.J., Kumar, G.R., Naidu, K.C.B., *Review on magnetocaloric effect and materials*, Journal of Superconductivity and Novel Magnetism, 31,1971-1979, 2018.

[12] Franco, V., Blázquez, J.S., Ipus, J.J., Law, J.Y., Moreno-Ramírez, L.M., Conde, A., *Magnetocaloric effect: from materials research to refrigeration devices*, Progress in Materials Science, 93, 112-232, 2018.

[13] Lyubina, J., *Magnetocaloric materials for energy efficient cooling*, Journal of Physics D: Applied Physics, 50, 53002-53002, 2017.

[14] Pecharsky, V.K., Gschneidner Jr, K.A., *Giant magnetocaloric effect in $Gd_5(Si_2Ge_2)$,* Physical Review Letters, 78, 4494-4497, 1997.

[15] Ayaş, A.O., Kandemir, A., Kılıç Çetin, S., Akça, G., Akyol, M., Ekicibil, A., *Investigation of the effect of sintering temperature on structural, magnetic and magnetocaloric properties in $PrCaMn_2O_6$ double perovskite manganite system*, Journal of Materials Science: Materials in Electronics, 33, 7357-7370, 2022.

[16] Kılıç Çetin, S., Akça, G., Ayaş, A.O., Akyol, M., Ekicibil, A., *Structural, magnetic, and magnetocaloric properties of pb-substituted $La_{0.7}(Te_{1-x}Pb_x)_{0.3}MnO_3$ $(0.0 \leq x \leq 0.3)$ manganites*, Journal of Superconductivity and Novel Magnetism, 33, 527-538, 2020.

[17] Ayaş, A.O., Kılıç Çetin, S., Akyol, M., Akça, G., Ekicibil, A., *Effect of B site partial Ru substitution on structural magnetic and magnetocaloric properties in $La_{0.7}Pb_{0.3}Mn_{1-x}Ru_xO_3$ (x = 0.0, 0.1 and 0.2) perovskite system*, Journal of Molecular Structure, 1200, 127120-127120, 2020.

[18] Kanıkırmızı, T., İzgi, T., Bayri, N., Gencer, H., Kolat, V.S., Pektas, M., Atalay, S., *Structural, magnetic and magnetocaloric properties of Ru doped $Pr_{0.67}Ca_{0.33}Mn_{1-x}Ru_xO_3$ manganites,* Journal of Materials Science: Materials in Electronics, 33, 21778-21795, 2022.

[19] Kılıç Çetin, S., Akça, G., Aslan, M.S., Ekicibil, A., *Role of nickel doping on magnetocaloric properties of $La_{0.7}Sr_{0.3} Mn_{1-x}Ni_xO_3$ manganites*, Journal of Materials Science: Materials in Electronics, 32, 10458-10472, 2021.

[20] Privitera, A., Righetto, M., Cacialli, F., Riede, M.K., *Perspectives of organic and perovskite-based spintronics*, Advanced Optical Materials, 9, 2100215, 2021.

[21] Balcells, L., Carrillo, A.E., Martínez, B., Sandiumenge, F., Fontcuberta, J., *Room temperature magnetoresistive sensor based on thick films manganese perovskite*, Journal of Magnetism and Magnetic Materials, 221, 224-230, 2000.

[22] Balcells, L., Fontcuberta, J., Martínez, B., Obradors, X., *High-field magnetoresistance at interfaces in manganese perovskites,* Physical Review B, 58, R14697-R14700, 1998.

[23] Barman, A., Kar-Narayan, S., Mukherjee, D., *Caloric effects in perovskite oxides*, Advanced Materials Interfaces, 6, 1900291-1900291, 2019.

[24] Ayaş, A.O., *Observation of room-temperature range magnetocaloric effect in $PrSr_{1-x}Pb_xMn_2O_6$ (0.4 ≤ x ≤ 0.6) double-perovskite manganite system*, Journal of Superconductivity and Novel Magnetism, 32, 393-403, 2019.

[25] Ayaş, A.O., *Structural and magnetic properties with reversible magnetocaloric effect in $PrSr_{1-x}Pb_xMn_2O_6$ (0.1 ≤ x ≤ 0.3) double perovskite manganite structures*, Philosophical Magazine, 98, 2782-2796, 2018.

[26] Akça, G., Ayaş, A.O., Kılıç Çetin, S., Akyol, M., Ekicibil, A., *Effect of monovalent cation doping on structural, magnetic, and magnetocaloric properties of $Pr_{0.85}A_{0.15}MnO_3$ (A = Ag and K) manganites*, Journal of Superconductivity and Novel Magnetism, 30, 1515-1525, 2017.

[27] Kılıç Çetin, S., Acet, M., Ekicibil, A., Sarıkürkçü, C., Kıymaç, K., *Reversibility in the adiabatic temperature-change of $Pr_{0.73}Pb_{0.27}MnO_3$*, Journal of Alloys and Compounds, 565, 139-143, 2013.

[28] Ayaş, A.O., Akyol, M., Kılıç Çetin, S., Kaya, M., Dinçer İ., Ekicibil, A., Elerman, Y., *Room temperature magnetocaloric effect in $Pr_{1.75}Sr_{1.25}Mn_2O_7$ double-layered perovskite manganite system*, Philosophical Magazine, 97, 671-682, 2017.

[29] Rietveld, H., *A profile refinement method for nuclear and magnetic structures*, Journal of Applied Crystallography, 2, 65-71, 1969.

[30] Rodríguez-Carvajal, J., *Recent advances in magnetic structure determination by neutron powder diffraction*, Physica B: Condensed Matter, 192, 55-69, 1993.

[31] Debye, P., Scherrer, P., *Interference on inordinate orientated particles in Roentgen light*, Physikalische Zeitschrift, 17, 277-283, 1996.

[32] Debye, P., Scherrer, P., *Interference on inordinate orientated particles in X-ray light III*, Physikalische Zeitschrift, 18, 291-301, 1997.

[33] Chandra, K., Singhal, S., Goyal, S., *Magnetic and Mössbauer spectral studies of nano crystalline cobalt substituted magnesium ferrites ($Mg_xCo_{1-x}Fe_2O_4$)*, Hyperfine Interactions, 183, 75-80, 2008.

[34] Rajendran, M., Pullar, R.C., Bhattacharya, A.K., Das, D., Chintalapudi, S.N., Majumdar, C.K., *Magnetic properties of nanocrystalline $CoFe_2O_4$ powders prepared at room temperature: variation with crystallite size*, Journal of Magnetism and Magnetic Materials, 232, 71-83, 2001.

[35] Barati, M.R., *Characterization and preparation of nanocrystalline MgCuZn ferrite powders synthesized by Sol–Gel Auto-Combustion Method*, Journal of Sol-Gel Science and Technology, 52, 171-178, 2009.

[36] Kumar, V., Rana, A., Yadav, M.S., Pant, R.P., *Size-induced effect on nano-crystalline $CoFe_2O_4$*, Journal of Magnetism and Magnetic Materials, 320, 1729-1734, 2008.

[37] Krishna Murthy, J., Devi Chandrasekhar, K., Mahana, S., Topwal, D., Venimadhav, A., *Giant magnetocaloric effect in Gd_2NiMnO_6 and Gd_2CoMnO_6 ferromagnetic insulators*, Journal of Physics D: Applied Physics, 48, 355001-355001, 2015.

[38] Phong, P.T., Manh, D.H., Hoan, L.C., Ngai, T.V., Phuc, N.X., Lee, I.-J., *Particle size effects on $La_{0.7}Ca_{0.3}MnO_3$: Griffiths phase-like behavior and magnetocaloric study*, Journal of Alloys and Compounds, 662, 557-565, 2016.

[39] Phong, P.T., Dang, N.V., Bau, L.V., An, N.M., Lee, I.-J., *Landau mean-field analysis and estimation of the spontaneous magnetization from magnetic entropy change in La$_{0.7}$Sr$_{0.3}$MnO$_3$ and La$_{0.7}$Sr$_{0.3}$Mn$_{0.95}$Ti$_{0.05}$O$_3$*, Journal of Alloys and Compounds, 698, 451-459, 2017.

[40] Banerjee, B.K., *On a Generalised approach to first and second order magnetic transitions,* Physics Letters, 12, 16-17, 1964.